

sorption results<sup>9</sup> revealed that the iron surface was mostly covered by promoter oxides of Al, Ca, and K. Postreaction XPS results also revealed a C(1s) XPS peak of weak to moderate intensity centered at 284.1–283.7 eV. This binding energy approaches those (ca. 283.5 eV) reported for iron carbides.<sup>4b,10</sup>

More convincing evidence for carbide formation was obtained from TPHT results collected after reaction studies like those displayed in Figure 1 in which methane was the only product. After reaction at temperatures below 340 °C, only small amounts of reactive carbon could be distinguished with maximum methane desorption rates near 300 °C. However, for higher reaction temperatures, large amounts of methane were produced with a maximum rate just above 400 °C. Since XPS results revealed only small amounts of carbonaceous residue on top of the catalyst surface, this reactive carbon must be associated with carbiding of the catalyst. Consequently, it appears that the active carbon incorporation catalyst is carbided iron. This conclusion is well supported by bulk carbon to iron stoichiometries of 0.1–0.25 estimated from the TPHT peak areas which were adequate to represent 40–60% conversion to bulk carbides such as Fe<sub>3</sub>C or Fe<sub>5</sub>C<sub>2</sub>. Moreover, preliminary results from studies using bona fide iron carbides have shown similar catalytic behavior.<sup>5</sup>

**Acknowledgment.** We acknowledge contributions by Mr. W. S. Varnado along with support of this research by the Exxon Research and Engineering Company.

(8) (a) Silverman, D. C.; Boudart, M. *J. Catal.* **1982**, *77*, 208. (b) Ertl, G.; Thiele, N. *Appl. Surf. Sci.* **1979**, *3*, 99. (c) Brunauer, S.; Emmett, P. H. *J. Am. Chem. Soc.* **1940**, *62*, 1732.

(9) Davis, S. M. *Catal. Lett.* **1988**, *1*, 85.

(10) (a) Dwyer, D. J.; Hardenbergh, J. H. *J. Catal.* **1984**, *87*, 66. (b) Bonzel, H. P.; Broden, G.; Krebs, H. J. *Appl. Surf. Sci.* **1983**, *16*, 373. (c) Bonzel, H. P.; Krebs, H. J. *Surf. Sci.* **1983**, *109*, L527.

## Semianalytical Treatment of Solvation for Molecular Mechanics and Dynamics

W. Clark Still,\* Anna Tempczyk, Ronald C. Hawley, and Thomas Hendrickson

Department of Chemistry, Columbia University  
New York, New York 10027

Received February 12, 1990

Dealing with solvent has been a perpetual problem for molecular modeling. While using explicit solvent molecules provides one solution to the problem, such calculations require a major computational effort if converged energies are required. Here we describe a more practical alternative in which solvent is treated as a statistical continuum.<sup>1</sup> The treatment provides both energies and derivatives analytically and thus may be used in a molecular mechanics force field. As we will show, it gives small-molecule hydration energies of comparable accuracy to those obtained from contemporary free energy perturbation methods but at only a fraction of the computational expense.

**Method.** We consider solvation free energy ( $G_{\text{sol}}$ ) traditionally as consisting of a solvent–solvent cavity term ( $G_{\text{cav}}$ ), a solute–solvent van der Waals term ( $G_{\text{vdW}}$ ), and a solute–solvent electrostatic polarization term ( $G_{\text{pol}}$ ):

$$G_{\text{sol}} = G_{\text{cav}} + G_{\text{vdW}} + G_{\text{pol}} \quad (1)$$

(1) Numerical methods of computing  $G_{\text{sol}}$  or  $G_{\text{pol}}$  using continuum models: (a) Eisenberg, D.; McLachlan, A. D. *Nature (London)* **1986**, *319*, 199. (b) Ooi, T.; Oobatake, M.; Nemethy, G.; Scheraga, H. A. *Proc. Natl. Acad. Sci. U.S.A.* **1987**, *84*, 3086. (c) Kang, Y. K.; Nemethy, G.; Scheraga, H. A. *J. Phys. Chem.* **1987**, *91*, 4105, 4109, 4118. (d) Warshel, A.; Russel, S. T. *Q. Rev. Biophys.* **1984**, *17*, 283. (e) Gilson, M.; Honig, B. *Proteins* **1988**, *4*, 7.

Noting that  $G_{\text{sol}}$  for the saturated hydrocarbons in water is linearly related<sup>2</sup> to solvent-accessible surface area (SA), we follow precedent<sup>1a,b</sup> by setting

$$G_{\text{cav}} + G_{\text{vdW}} = \sum \sigma_k \text{SA}_k \quad (2)$$

where  $\text{SA}_k$  is the total solvent-accessible surface area of atoms of type  $k$  and  $\sigma_k$  is an empirical atomic solvation parameter. As a preliminary value for  $\sigma_k$ , we use +7.2 cal/(mol Å<sup>2</sup>) for all atom types to reproduce hydration energies of simple hydrocarbons using our recently described analytical surface area calculation.<sup>3</sup>

For  $G_{\text{pol}}$ , the total electrostatic free energy ( $G_{\text{es}}$ , kcal/mol) of a system of widely separated particles (separations  $r$  (Å), charges  $q$  (electrons), radii  $\alpha$  (Å)) in a medium of dielectric constant  $\epsilon$  is given (eq 3) by the sum of Coulomb's law in a dielectric (term 1) and the Born equation (term 2). Term 1 can be expanded algebraically (eq 4) to give Coulomb's law in vacuo and a new second term which accounts for the effect of the dielectric medium on the pairwise interactions of charged particles. The sum of terms 2 and 3 in eq 4 is equal to  $G_{\text{pol}}$  and has been termed the generalized Born (GB) equation.<sup>4</sup> The similar form of terms 2 and 3 in eq

$$G_{\text{es}} = 332 \sum_{i=1}^{n-1} \sum_{j=i+1}^n \frac{q_i q_j}{r_{ij} \epsilon} - 166 \left(1 - \frac{1}{\epsilon}\right) \sum_i \frac{q_i^2}{\alpha_i} \quad (3)$$

$$= 332 \sum_{i=1}^{n-1} \sum_{j=i+1}^n \frac{q_i q_j}{r_{ij}} - 332 \left(1 - \frac{1}{\epsilon}\right) \sum_{i=1}^{n-1} \sum_{j=i+1}^n \frac{q_i q_j}{r_{ij}} - 166 \left(1 - \frac{1}{\epsilon}\right) \sum_i \frac{q_i^2}{\alpha_i} \quad (4)$$

$$G_{\text{pol}} = -166 \left(1 - \frac{1}{\epsilon}\right) \sum_{i=1}^n \sum_{j=1}^n \frac{q_i q_j}{f_{\text{GB}}} \quad (5)$$

4 prompts us to combine them into a single expression (eq 5) where we define  $f_{\text{GB}}$  as a function of  $r_{ij}$  and  $\alpha_i$  which makes eq 5 mimic the relevant equations of classical electrostatics. While we have not defined  $f_{\text{GB}}$  uniquely, one simple but effective expression is  $f_{\text{GB}} = (r_{ij}^2 + \alpha_{ij}^2 e^{-D})^{0.5}$  where  $\alpha_{ij} = (\alpha_i \alpha_j)^{0.5}$  and  $D = r_{ij}^2 / (2\alpha_{ij}^2)$ . Used in eq 5, this expression gives the Born equation for superimposed charges when  $r_{ij} = 0$ , the Onsager reaction field energy within 10% for a dipole in a spherical cavity when  $r_{ij} < 0.1\alpha_{ij}$ , and the Born + Coulomb dielectric polarization energy within 1% for two charged spheres when  $r_{ij} > 2.5\alpha_{ij}$ . It is superior to eq 4, which overestimates the interaction of buried charges with the dielectric, and to  $f_{\text{GB}} = (r_{ij}^2 + \alpha_{ij}^2)^{0.5}$ , which underestimates the corresponding interaction of proximate exposed charges.

We compute Born radii ( $\alpha_i$ ) numerically for each charged atom  $i$  in the solute. This is done by evaluating  $G_{\text{pol}(i)}$  for each such atom with a continuum dielectric medium using a finite difference method (see supplementary material) assuming that all other atoms are neutral and displace the dielectric. Given  $G_{\text{pol}(i)}$ , the effective spherical Born radius is obtained by solving the Born term of eq 3 ( $n = 1$ ) for  $\alpha_i$ . We take the dielectric to begin at some fixed, solvent-dependent distance from the solute van der Waals surface.<sup>5</sup> For water solvent and atomic radii taken from the OPLS force field,<sup>6</sup> we established this dielectric offset empirically as  $-0.09$  Å. We calculate derivatives of eq 5 treating  $\alpha_i$  as a constant which can be updated periodically along with the nonbonded pairlist. In the absence of major conformational changes, the simplification of a constant  $\alpha$  does not introduce large errors because  $f_{\text{GB}}$  is  $\sim 10$  times more sensitive to small changes in  $r_{ij}$  than to the associated changes in  $\alpha_{ij}$ .

(2) Hermann, R. B. *J. Phys. Chem.* **1972**, *76*, 2754. Amidon, G. L.; Yalkowsky, S. H.; Anik, S. T.; Valvani, S. C. *J. Phys. Chem.* **1975**, *72*, 2239. See also: Floris, F.; Tomasi, J. *J. Comput. Chem.* **1989**, *10*, 616.

(3) Hasel, W.; Hendrickson, T. F.; Still, W. C. *Tetrahedron Comput. Methodol.* **1988**, *1*, 103.

(4) Constanciel, R.; Contreras, R. *Theor. Chim. Acta* **1984**, *65*, 1. Kozaki, T.; Morihashi, K.; Kikuchi, O. *J. Mol. Struct.* **1988**, *168*, 265. Kozaki, T.; Morihashi, K.; Kikuchi, O. *J. Am. Chem. Soc.* **1989**, *111*, 1547 and references therein. See also: Goodford, P. J. *J. Med. Chem.* **1985**, *28*, 849.

(5) Cf.: Rashin, A. A.; Honig, B. *J. Phys. Chem.* **1985**, *89*, 5588.

(6) Jorgensen, W. L.; Tirado-Rives, J. *J. Am. Chem. Soc.* **1988**, *110*, 1657. For hydrogens bound to heteroatoms, we used the OPLS radius of 0.0 in our FEP calculations whereas we used a radius of 1.15 Å in eq 5. For other atoms, we took  $0.5\sigma$  as van der Waals radii. We thank Professor Jorgensen for his most recent set of OPLS parameters.

**Table I.** Comparison of Solvation Free Energies from Eqs 2 and 5 with FEP Calculations and Experiment

solute	$G_{\text{pol}}$ , kcal/mol		$G_{\text{sol}}$ , kcal/mol	
	FEP <sup>a</sup>	eq 5 <sup>e</sup>	expt <sup>a</sup>	eqs 2 + 5 <sup>f</sup>
methanol	-7.1 ± 0.3	-7.1	-5.1 <sup>b,d</sup>	-6.2
ethanol	-7.4 ± 0.2	-6.4	-5.0 <sup>b</sup>	-5.2
2-propanol	-7.1 ± 0.3	-5.7	-4.8 <sup>b</sup>	-4.3
acetone	-4.5 ± 0.2	-4.7	-3.9, <sup>b</sup> -3.8 <sup>d</sup>	-3.2
dimethyl ether			-1.9 <sup>b</sup>	-2.0
methyl acetate	-3.1 ± 0.2	-3.9	-3.3 <sup>b</sup>	-2.2
acetic acid	-6.8 ± 0.3	-7.7	-6.7 <sup>b,d</sup>	-6.5
<i>N,N</i> -dimethylacetamide	-7.5 ± 0.5	-7.3		
acetamide	-10.8 ± 0.5	-11.4	-9.7 <sup>b</sup>	-10.6
( <i>Z</i> )- <i>N</i> -methylacetamide	-10.1 ± 0.5	-9.0		
( <i>E</i> )- <i>N</i> -methylacetamide	-7.4 ± 0.6	-7.5		
( <i>E</i> )- <i>N</i> -methylacetamide dimer	-4.6 ± 0.2	-5.3		
alanine dipeptide (C7 <sub>eq</sub> )	-13.1 ± 0.4	-12.2		
alanine dipeptide (C5)	-12.3 ± 0.5	-12.4		
alanine dipeptide ( $\alpha_R$ )	-20.9 ± 0.7	-18.9		
acetonitrile			-3.9 <sup>d</sup>	-4.8
methyl mercaptan			-1.2, <sup>b</sup> -1.3 <sup>d</sup>	-3.3
benzene	-1.9 ± 0.3	-2.6	-0.9, <sup>b</sup> 0.8 <sup>c</sup>	-1.0
toluene	-0.7 ± 0.2	-1.9	-0.9, <sup>b</sup> -0.8 <sup>c</sup>	-0.1
phenol	-8.0 ± 0.7	-7.7	-6.6 <sup>b</sup>	-6.3
pyridine			-4.7 <sup>d</sup>	-4.4
imidazole			-5.9 <sup>d,h</sup>	-6.5
ammonium ion	-103.9 <sup>g</sup> ± 0.7	-91.2	-79 <sup>d</sup>	-90.8
methylammonium ion			-71, <sup>b</sup> -70 <sup>d</sup>	-80.4
trimethylammonium ion			-59 <sup>d</sup>	-63.1
acetate ion	-91.3 <sup>g</sup> ± 1.4	-83.7	-80, <sup>b</sup> -77 <sup>d</sup>	-82.9
ammonium acetate	-47.7 ± 0.9	-43.1		
ethane		0.0	+1.8, <sup>c</sup> ±2.1 <sup>d</sup>	+1.3
<i>n</i> -butane (anti)		0.0	+2.3 <sup>c</sup>	+1.9
<i>n</i> -hexane (all anti)		0.0	+2.6 <sup>c</sup>	+2.4
cyclohexane (chair)		0.0	+1.2 <sup>c</sup>	+1.8
<i>N</i> -octane (all anti)		0.0	+2.9 <sup>c</sup>	+2.9

<sup>a</sup> Free energy of transfer from 1 M ideal gas state to 1 M ideal aqueous solution at 25 °C. <sup>b</sup> Cabani, S.; Gianni, P.; Mollica, V.; Lepori, L. *J. Solution Chem.* **1981**, *10*, 563. <sup>c</sup> Ben-Naim, A.; Marcus, Y. *J. Chem. Phys.* **1984**, *81*, 2016. <sup>d</sup> Pearson, R. G. *J. Am. Chem. Soc.* **1986**, *108*, 6109. <sup>e</sup> Geometries obtained by energy minimization in vacuo. <sup>f</sup> Geometries obtained by energy minimization in eqs 2 + 5 water. <sup>g</sup> Value includes a -19.3 kcal/mol Born correction for the 8.5-Å solute-solvent cutoffs employed (Jorgensen, W. L.; Blake, J. F.; Buckner, J. K. *Chem. Phys.* **1989**, *129*, 193). <sup>h</sup> Estimated energy.

**Results.** To test eq 5, we compared its values for  $G_{\text{pol}}$  using  $\epsilon = 78.3$  for a series of small-molecule solutes with those from free energy perturbation (FEP) calculations.<sup>7</sup> In the FEP calculations,<sup>8</sup> the perturbations consisted of electrically charging and discharging the solutes in a bath of TIP4P water molecules. Except for hydrogen radii, the same nonbonded parameters (atomic charges and radii) were used in both the FEP and eq 5 calculations, and these were taken from the OPLS force field.<sup>6</sup> The results are given in Table I. Taking the  $G_{\text{pol}}$  data for neutral molecules, we found a linear correlation (slope = 1.1, correlation coefficient  $r^2 = 0.98$ ) between the results of FEP and eq 5. Although FEP on  $\text{NH}_4^+$  and  $\text{AcO}^-$  gives  $G_{\text{pol}}$  more negative than does eq 5, the FEP values are also more negative than experimental  $G_{\text{sol}}$  by 10–20 kcal/mol. Thus  $G_{\text{pol}}$  has similar values for small molecules whether calculated by FEP using an explicit, molecular solvent or by our continuum model.

In Table I we also compare total solvation energies ( $G_{\text{sol}}$ ) found by experiment with those from eqs 2 and 5. Here too the correlation is linear (slope = 0.96,  $r^2 = 0.96$ ). The correlation is illustrated in Figure 1, which plots the neutral molecule  $G_{\text{sol}}$  data from Table I. Even for ions, the model performs well and gives aqueous 1 M  $\text{NH}_4\text{OAc}$  as dissociated in spite of the ~130 kcal/mol attraction between the ions in vacuo.  $G_{\text{pol}}$  is sensitive to the partial charges used. For example, only a 10% reduction in the OPLS charges of MeSH was required to lower  $G_{\text{pol}}$  by ~0.9 kcal/mol and bring  $G_{\text{sol}}$  to within 1.2 kcal/mol of experiment. Thus solvation free energies are calculated reliably only when accurate atomic partial charges are used.

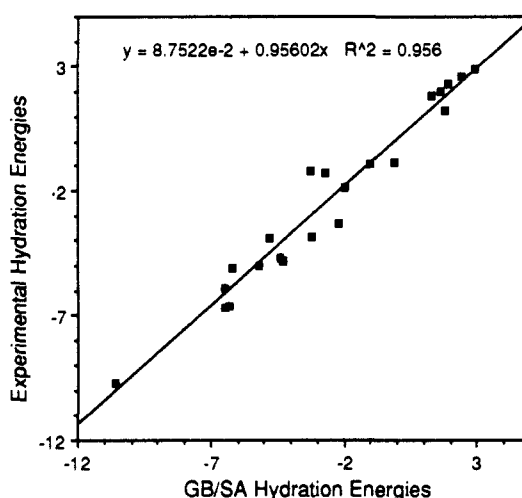


**Figure 1.** Comparison of experimental free energies of solvation in water (kcal/mol) for neutral small molecules with GB/SA energies calculated by using eqs 2 and 5.

Given that the GB/SA solvation treatment described here requires adding only two new parameters ( $\sigma$  in eq 2 and the dielectric offset used to compute  $\alpha$  in eq 5) to those in an existing force field, the correlation between our results and experiments or molecular solvent calculations is remarkable. Using analytical derivatives of eqs 2 and 5, we are able to carry out converged molecular mechanics or dynamics with only 2–4-fold reduction in speed over corresponding in vacuo calculations. In comparison with a single FEP calculation of  $\Delta G_{\text{sol}}$  which requires several weeks of MicroVAX 3200 computer time, all 49 of the GB/SA calculations reported here were carried out within a total of 1 cpu min. The solvation treatment described should provide a major advance

(7) Jorgensen, W. L. *Acc. Chem. Res.* **1989**, *22*, 184. van Gunsteren, W. F.; Berendsen, H. J. C. *J. Comput.-Aided Mol. Des.* **1987**, *1*, 171. Mezie, M.; Beveridge, D. L. *Ann. N.Y. Acad. Sci.* **1987**, *482*, 1.

(8) Carried out by using BOSS V2.0. W. L. Jorgensen, Department of Chemistry, Purdue University, West Lafayette, IN 47907.

in our ability to predict the properties of polar molecules in solution.<sup>9</sup>

**Supplementary Material Available:** Appendices describing the calculation of effective Born radii ( $\alpha$ ) and approximate surface areas (SA) (4 pages). Ordering information is given on any current masthead page.

(9) W.C.S. acknowledges the support of NSF Grant CHE89 11008. R.C.H. acknowledges the support of NIH National Research Service Award GM 13106. We also thank Professor Barry Honig for helpful discussions of electrostatic solvation.

## Surface Concentrations and Residence Times of Intermediates on $\text{Sm}_2\text{O}_3$ during the Oxidative Coupling of Methane

K. P. Peil, J. G. Goodwin, Jr.,\* and G. Marcelin

Department of Chemical and Petroleum Engineering  
University of Pittsburgh, Pittsburgh, Pennsylvania 15261

Received September 12, 1989

Revised Manuscript Received April 24, 1990

The use of  $\text{Sm}_2\text{O}_3$  as a catalyst for the oxidative coupling of methane has been well studied and documented.<sup>1-3</sup> However, detailed information on the surface of a working  $\text{Sm}_2\text{O}_3$  catalyst and the overall carbon reaction pathway is unknown. This communication presents results that delineate completely for the first time the nature of the surface-reaction steps of  $\text{Sm}_2\text{O}_3$  and quantifies the working surface under steady-state reaction conditions.

The feasibility of using isotope switching experiments to study oxidative methane coupling has recently been shown.<sup>4-6</sup> Some of the conclusions drawn from these experiments include the participation of the lattice oxygen in the reaction along with significant surface holdup of the methane and  $\text{CO}_x$  products. However, it is difficult to obtain quantitative results from the majority of this work<sup>5,6</sup> due to the pulsing technique employed.<sup>7</sup>

The technique used in this study involved switching the isotopic composition of methane from  $^{12}\text{CH}_4$  to  $^{13}\text{CH}_4$  once the reaction had reached a steady state and subsequently following (by mass spectrometry) the evolution and decay of the different labeled reactants and products to their new steady-state values. Use of such a technique allowed the determination of surface coverages and intrinsic site activities as well as reaction pathways.<sup>4</sup>

The  $\text{Sm}_2\text{O}_3$  (BET surface area =  $1 \text{ m}^2/\text{g}$ ) was purchased from Alfa Products. Prior to reaction, it was pretreated by heating to reaction temperature in flowing oxygen and then holding at reaction temperature for 30 min prior to introduction of the reactants. The reaction conditions used in this work were as follows: catalyst weight = 100 mg; temperature = 600 °C; total pressure = 1 atm;  $\text{CH}_4$  flow =  $5 \text{ cm}^3/\text{min}$ ;  $\text{He}/\text{CH}_4/\text{O}_2 = 94/10/1$ . These conditions resulted in a  $\text{CH}_4$  conversion of 9.1%, a  $\text{CO}_2/\text{CO}$  ratio of 1.4, and a  $\text{C}_2$  selectivity of 25.7%. A straight-tube quartz reactor was used with an inlet i.d. of 4 mm which tapered to 1 mm after the catalyst bed. The catalyst bed was held in place by quartz wool, and in the absence of any catalyst the quartz reactor and quartz wool had negligible activity.

Figure 1 presents the transients obtained when the isotopic composition of methane is switched as described above. A trace amount of argon was present in one of the methane isotopes, which permitted correction for gas-phase holdup. The rapid relaxation

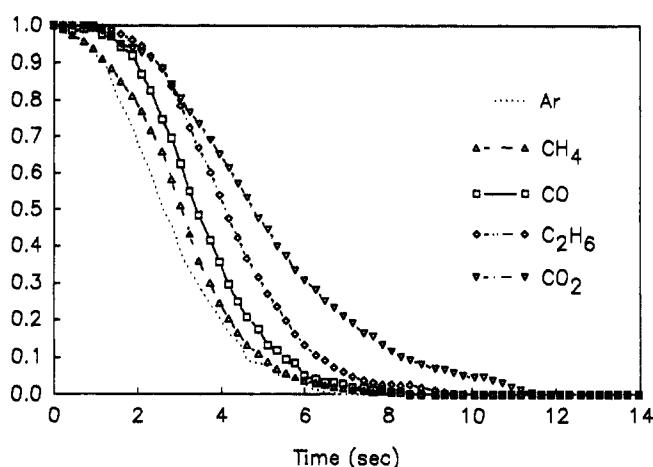


**Figure 1.** Carbon transients for the oxidative coupling of methane over  $\text{Sm}_2\text{O}_3$ . Each transient is the average of three separate experiments. The dotted line indicates an inert-gas tracer.

**Table I.** Surface Residence Times along the Carbon Reaction Pathway as a Function of Catalyst Loading

species	surf. residence time of C, <sup>a</sup> s		
	25 mg	45 mg	100 mg
$\text{C}_2\text{H}_6$	$4.0 \pm 0.7$	$4.1 \pm 0.7$	$2.8 \pm 0.7$
$\text{CO}_2$	2.7	3.4	2.7
CO	2.3	2.4	1.7

<sup>a</sup>Data collection for Table I permitted the collection of only five or six data points per transient response, yielding the relatively large potential error of  $\pm 0.7 \text{ s}$ .

of the methane signal indicates the lack of a long-lived adsorbed methane. This result is consistent with a similar observation made with the Li/MgO system<sup>4</sup> and in direct contrast with the results of Ekstrom and Lapszewicz.<sup>5,6</sup> This difference appears to be due to diffusion effects in the higher surface area and higher porosity  $\text{Sm}_2\text{O}_3$  which was used by Ekstrom and Lapszewicz.<sup>8</sup> When using high-porosity catalysts, we observed isotopic transients with significant tailing, similar to those reported by Ekstrom and Lapszewicz.

The fact that the  $\text{CO}_2$  transient trails the CO transient may suggest a possible multistep surface oxidation pathway. However, the possibility that  $\text{CO}_2$  is formed as a primary product and not from further oxidation of adsorbed CO cannot be completely ruled out from this data. The lack of strongly adsorbed  $\text{CO}_2$  is evident from the rapid relaxation of the  $\text{CO}_2$  transient. This observation has been confirmed by a series of experiments in which the catalyst bed length was varied, resulting in no change (within experimental error) in the  $\text{CO}_2$  residence time, indicating that readsorption of  $\text{CO}_2$  was not important (see Table I). Although the surface residence times presented in Table I are subject to a relatively large error of approximately 0.7 s, they clearly show the lack of any relationship between catalyst bed length and surface residence time. Hence, no significant readsorption of any of the product molecules is indicated. By contrast, a similar set of measurements for  $\text{CO}_2$  over a Li/MgO catalyst, which is known to form carbonates easily, indicated a 2-fold increase in residence time for  $\text{CO}_2$  with a 2-fold increase in the amount of catalyst.<sup>9</sup>

These results are consistent with reports indicating that  $\text{Sm}_2(\text{CO}_3)_3$  is stable up to only 600 °C in an atmosphere void of  $\text{CO}_2$  and to 850 °C in 500 Torr of  $\text{CO}_2$ .<sup>10</sup> Under the conditions employed in this study, only 2.8 Torr of  $\text{CO}_2$  was present. Therefore, surface carbonates would not be expected to be very stable or present in any large amounts under the reaction conditions used for this study.

\* To whom all correspondence should be addressed.

(1) Otsuka, K.; Jinno, K.; Morikawa, A. *J. Catal.* **1986**, *100*, 353.

(2) Otsuka, K.; Jinno, K.; Morikawa, A. *Chem. Lett.* **1985**, 499.

(3) Otsuka, K.; Jinno, K.; Morikawa, A. *Chem. Lett.* **1987**, 483.

(4) Peil, K. P.; Goodwin, J. G., Jr.; Marcelin, G. *J. Phys. Chem.* **1989**, *93*, 5977.

(5) Ekstrom, A.; Lapszewicz, J. A. *J. Am. Chem. Soc.* **1988**, *110*, 5226.

(6) Ekstrom, A.; Lapszewicz, J. A. *J. Phys. Chem.* **1989**, *93*, 5230.

(7) Soong, Y.; Krishna, K.; Biloen, P. *J. Catal.* **1986**, *97*, 330.

(8) Ekstrom, A., private communication.

(9) Peil, K. P.; Goodwin, J. G., Jr.; Marcelin, G. Manuscript submitted for publication.

(10) *Rare Earth Research II*; Vorres, K. S., Ed.; Science Publishers: New York, 1964.